J. Phys.: Condens. Matter **12** (2000) 375–397. Printed in the UK PII: S0953-8984(00)07189-7

A molecular dynamical investigation of high pressure phase transformations in berlinite (α-$AlPO_4$)

Nandini Garg and Surinder M Sharma

Condensed Matter Physics Division, Bhabha Atomic Research Centre, Mumbai 400 085, India

Received 24 August 1999, in final form 28 October 1999

Abstract. Since 1990, berlinite (α-$AlPO_4$) has been believed to have a memory glass property under high pressures. Recent high pressure Raman scattering experiments have raised serious doubts in our understanding of the high pressure behaviour of α-$AlPO_4$. We have now carried out extensive molecular dynamical calculations to understand the nature of structural changes in α-$AlPO_4$ under high pressures. Our simulations show that around 15 GPa the oxygen sublattice becomes disordered and the intensities of the Bragg diffraction peaks are reduced. High pressure causes a monotonic increase in the distortion of the AlO_4 and PO_4 tetrahedra; and, as observed in earlier MD calculations, α-$AlPO_4$ undergoes a first order phase transformation at $\sim$30 GPa to a disordered structure. However, even beyond 30 GPa, the calculated diffraction pattern of this phase continues to show sharp diffraction peaks. At higher compression, this diffraction pattern shows a systematic reduction in the intensity and beyond 45 GPa, most of the peaks vanish except $(10\bar{1}2)$ and $(10\bar{1}4)$. These calculations show the persistence of translational order well beyond the generally accepted pressure of amorphization and support the recent Raman scattering results. Further, this disordered phase does not transform to any new crystalline phase on annealing at high pressures. Our simulations employing instantaneous compression confirm the earlier result that, beyond 12 GPa, the $Cmcm$ phase is more stable than the α-phase. However, this phase transforms to a four coordinated disordered phase at ambient conditions and can only be stabilized on compression beyond 20 GPa. Our results, presented here, strongly suggest the need for a re-investigation of α-$AlPO_4$ by x-ray diffraction under high pressures.

1. Introduction

Berlinite $AlPO_4$ exists in the α-quartz structure at ambient conditions and like quartz, it is reported to become amorphous at high pressures [1–7]. However, in $AlPO_4$, this transformation is reversible and the high pressure amorphous phase has been termed as a memory glass [1], as on the release of pressure the amorphous phase transforms back to the single crystal with the same orientations. In addition to the memory effect mentioned above, Brillouin scattering results suggest that the high pressure amorphous phase (p-glass [7]) is anisotropic [6]. Over the years there have been several theoretical investigations to understand these results [8–12]. Energy minimization and lattice dynamical calculations have suggested that, as in quartz, the oxygen atoms in α-$AlPO_4$ too have a tendency to approach the bcc lattice. These calculations [8, 9, 12] also showed that a zone boundary phonon mode along with a part of the acoustic branch softens at $\sim$30 GPa, and the softening of these modes was suggested to be responsible for the crystal to amorphous phase transformation [8, 9, 12]. Molecular dynamical (MD) calculations [10–12] have provided a significant insight into the reversibility of the crystal to amorphous transformation in $AlPO_4$. In particular, Tse and Klug [11] found that with increasing pressure, the spiralling AlO_4 and PO_4 tetrahedra

0953-8984/00/040375+23$30.00

distort and rotate into empty spaces in the crystal. This results in higher Al–O coordination. However, except at very high pressures, the phosphorus atoms predominantly retain fourfold coordination. On release of pressure, the oxygens around Al atoms relax back to the PO_4 tetrahedra which in turn displaces Al atoms back to their initial positions. Chaplot and Sikka [12] also obtained similar results and in addition showed that beyond 12 GPa enthalpy considerations favour an orthorhombic crystalline phase with $InPO_4$ structure (space group *Cmcm*). However, in the MD calculations α-$AlPO_4$ did not transform to the *Cmcm* phase at high pressures and this was suggested to be due to a free energy barrier prohibiting this phase transformation.

A few more experimental results have been reported since after the calculation mentioned above. A careful Raman scattering study by Gillet *et al* [13] extended the results of Jayaraman *et al* [14] who had observed an abrupt loss of Raman signal around 12 GPa. In contrast, Gillet *et al* observed that at $\sim$14 GPa, new Raman bands emerge along with the reduction in the intensity of Raman modes of α-$AlPO_4$. From these experimental results they argued that the memory effect is due to a crystalline–crystalline phase transition at this pressure and that the high pressure *crystalline phase is disordered*. Other Raman studies [15] also showed that under better hydrostatic conditions, α-$AlPO_4$ may not amorphize up to $\sim$30 GPa. In addition to these Raman investigations, Kruger and Meade [16] studied α-$AlPO_4$ with x-ray diffraction and reported a new phase at 6.5 GPa. A high resolution single crystal x-ray diffraction investigation by Sun *et al* [17] suggested the existence of a disordered crystalline phase at $\sim$12 GPa. Also recent experimental studies on isostructural α-$FePO_4$ and α-$GaPO_4$ showed that at higher pressures, these materials transform to a stable crystalline $InPO_4$ structure in the *Cmcm* space group [18–20]. Therefore, it would be interesting to search for a similar phase transformation in α-$AlPO_4$ also. To summarize, under hydrostatic pressures there are three issues [21] which need careful theoretical investigations.

(1) The structure of $AlPO_4$ beyond $\sim$15 GPa at 300 K.
(2) Does α-$AlPO_4$ become amorphous at high pressures, say beyond 30 GPa?
(3) Does α-$AlPO_4$ transform to the *Cmcm* or any other crystalline phase at high pressures or at high pressures and high temperatures?

To investigate all these issues, detailed MD calculations have been carried out and are presented here.

Before we present our results, we also note here that earlier MD calculations were carried out with relatively small number of atoms, e.g., 720 atoms by Vessal [10], 576 atoms by Tse and Klug [11] and 276 atoms by Chaplot and Sikka [12]. As most MD calculations use periodic boundary conditions, these small numbers of atoms limit the observation of any superstructure of the α-phase such as brought about by softening of the $1/3(110)$ zone boundary phonon mode [8, 9, 12]. Therefore we have carried out present calculations on a larger cell employing 2592 atoms. We may also note that earlier calculations suggested that the disagreement between the calculated ($\sim$30 GPa [10–12]) and the observed pressures (12–18 GPa [1, 2]) of amorphization may be due to inadequate optimization of inter-atomic pair potentials [11, 12]. Alternatively this mismatch was ascribed to the fact that MD simulations assume a perfect crystalline order while in reality the crystal may have defects [10]. In view of the fact that recent experiments indicate that amorphization, if at all, occurs at pressures higher than 30 GPa, we feel that the reservations about the pair potentials of van Beest *et al* [22] may be exaggerated. Therefore we have used the optimized pair potentials determined by van Beest *et al*, as these reproduce various bulk properties of polymorphs of $AlPO_n$ such as elastic moduli and lattice constants etc [22].

2. Computational details

We have performed molecular dynamical simulations using the DL_ POLY package for molecular simulations [23]. In our calculations we employed the NPT ensemble incorporating the Melchionna [24] modifications of the Nosé-Hoover algorithm [25]. The value of the time step was chosen to be 2 fs. Equilibration was evaluated by observing fluctuations of averages of volume, pressure and temperature. We used a MD cell of $6 \times 6 \times 4$ unit cells having 432 formula units of $AlPO_4$ for the α-phase. The initial state was generated using experimentally determined structural parameters [26] in the space group $P3_121$. For the orthorhombic $Cmcm$ phase the fractional coordinates were taken as those of $VCrO_4$ [27]. However, the lattice constants were chosen to have the same initial volume per formula unit as that of the α-$AlPO_4$ at 0.1 MPa at 300 K. For this phase we used a MD cell of $6 \times 6 \times 4$ unit cells having 576 formula units (3456 atoms). Most calculations were carried out at 300 K except when specified. Whenever the temperature was raised it was kept below 3000 K to ensure that the material does not show melting. Typically we equilibrated our system at each pressure for ∼24 ps and the final atomic coordinates were obtained after averaging for ∼6 ps. However, across a phase transformation, the coordinates had to be equilibrated for a longer duration. For example, across 30 GPa, the coordinates were equilibrated for ∼70 ps before averaging.

We carried out the following simulations to address the various issues mentioned in section 1.

(1) Pressure loading up to 65 GPa; up to 30 GPa in steps of 1 GPa and beyond that in steps of 5 GPa.
(2) Increase of temperature to ∼2000 K at 20 GPa.
(3) Increase of temperature to ∼2000 K at 45 GPa.
(4) Simulation of $AlPO_4$ in the $Cmcm$ phase up to 65 GPa. Heating of this system at 20 GPa to ∼2800 K.
(5) Sudden pressure loading of $AlPO_4$ in the $Cmcm$ phase to 20 GPa and subsequent increase of pressure to 85 GPa in steps of 5 GPa.

3. Results

This section is organized in two parts. In the first part, we summarize our results in the context of new experimental observations on α-$AlPO_4$. In the second part, we present our findings which evaluate the possibility of a phase transformation of α-$AlPO_4$ to another crystalline phase such as the $Cmcm$ phase.

3.1. MD simulations of α-AlPO$_4$

3.1.1. α-AlPO$_4$ under compression. α-$AlPO_4$ was equilibrated at 0.1 MPa and 300 K. Our equilibrated final volume per unit cell of 80.1 Å^3 compares well with the experimental value of 77.2 Å^3. This equilibrated structure was subjected sequentially to higher pressures as mentioned in step (1) of section 2. Calculated P–V/V_0 behaviour is shown in figure 1. This figure shows that the berlinite phase undergoes a first order phase transformation (P_{tr}) at 30 GPa with a 4% volume drop. This is in agreement with the earlier simulations of Vessal [10] ($P_{tr} = 33$ GPa; $\Delta V = 5\%$), Tse and Klug [11] ($P_{tr} = 31$ GPa, $\Delta V = 4\%$) and Chaplot and Sikka [12] ($P_{tr} = 30$ GPa, $\Delta V = 5\%$). A slight variation in the P_{tr} may be due to the differences in the chosen dimensions of the MD cell [9]. Below 30 GPa, an unconstrained fit to the Murnaghan equation of state gives $K_0 = 34.7$ GPa and $K_0' = 6$. This may be compared with the bulk modulus of 31.7 GPa calculated from the known elastic stiffness constants of

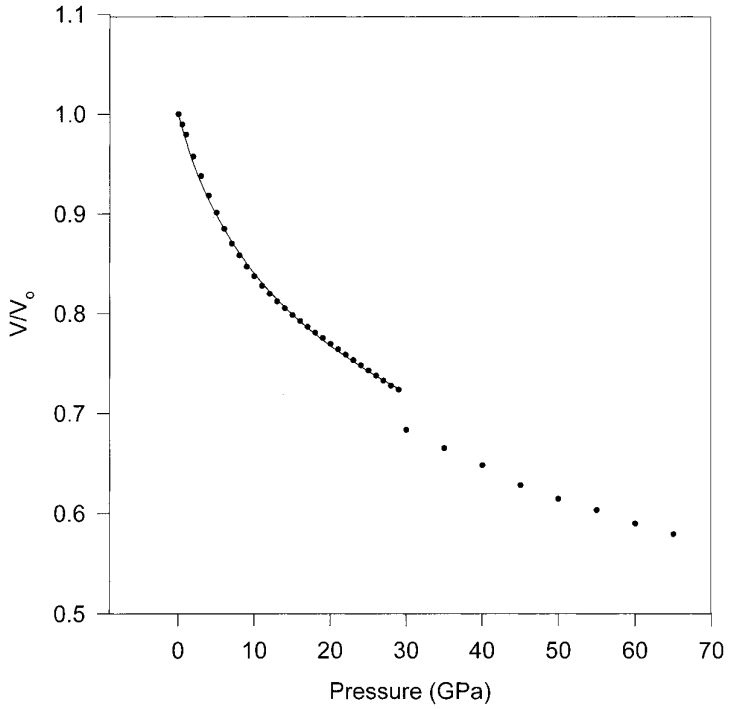

Figure 1. Calculated variation of V/V_0 as a function of pressure of berlinite. The solid line up to 30 GPa represents the fit to the Murnaghan equation of state with $K_0 = 34.7$ GPa and $K_0' = 6$.

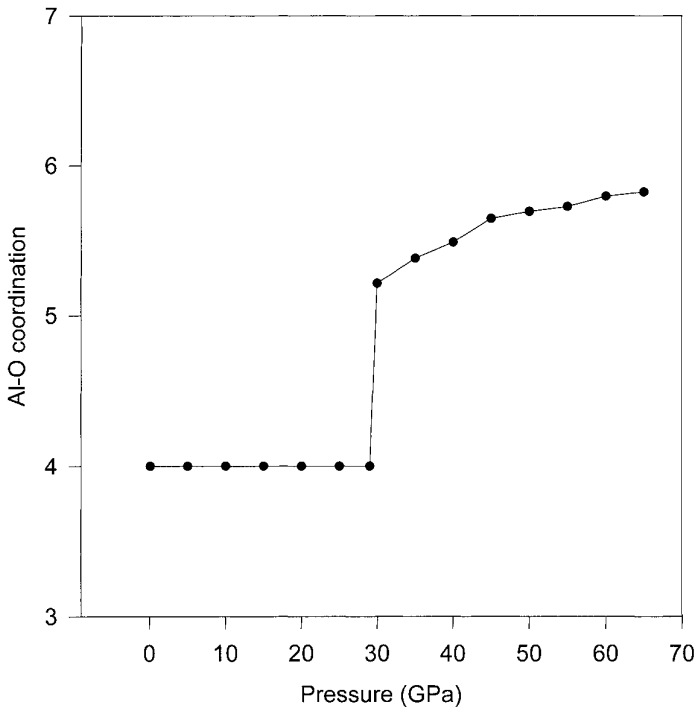

Figure 2. Variation of Al–O coordination as a function of pressure.

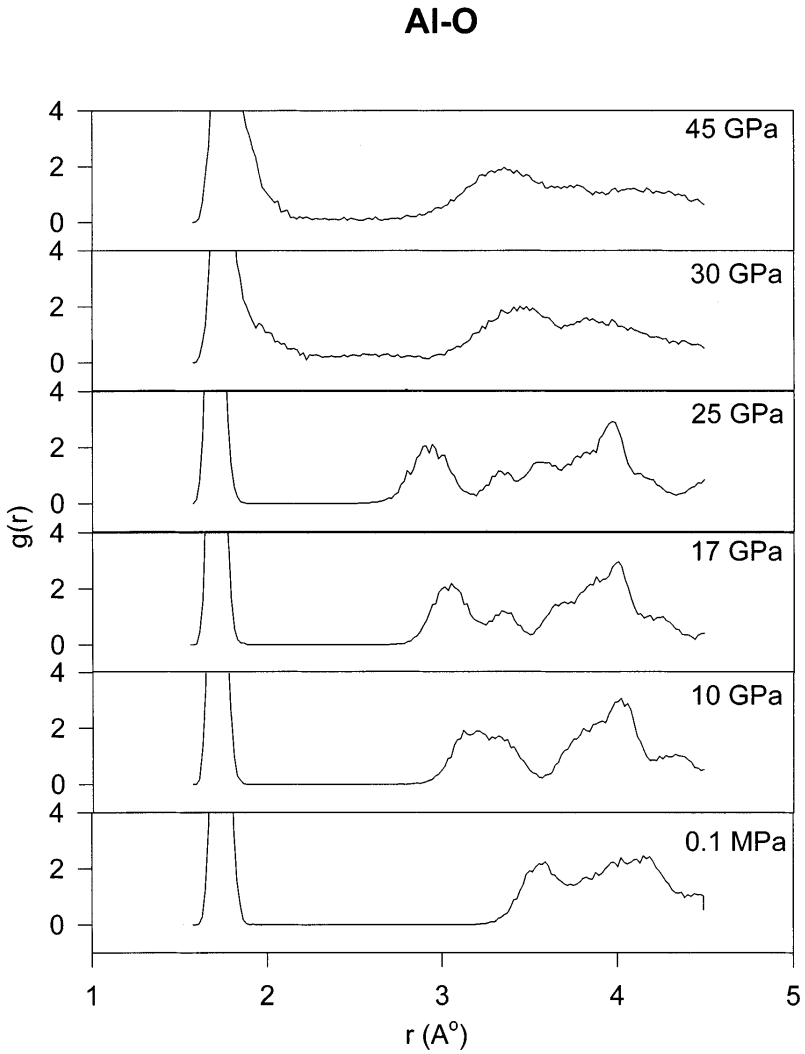

Figure 3. (a) Radial distribution function $g(r)$ for Al–O at various pressures. (The scale in these figures is so chosen to highlight reorganization of atoms beyond the nearest neighbours.) (b) Radial distribution function $g(r)$ for P–O at various pressures. (c) Radial distribution function $g(r)$ for O–O at various pressures.

α-AlPO$_4$ [28] and also with the experimental value of $K_0 = 36$ GPa and $K_0' = 4$ determined from the x-ray diffraction results [29].

Both Al and P continue to be four coordinated to the neighbouring oxygens up to a pressure of ∼30 GPa, in agreement with the results of Tse and Klug [11] and Chaplot and Sikka [12] but at variance with those of Vessal [10]. Vessal had found that even at ∼15 GPa, there are almost an equal number of Al atoms which are four and five coordinated to oxygens. Also, as in earlier simulations [10–12], we find a discontinuous change in Al–O coordination beyond 30 GPa. Variation of Al–O coordination, as a function of pressure is shown in figure 2. This coordination number was determined at a distance of the minimum between the first and second peak of

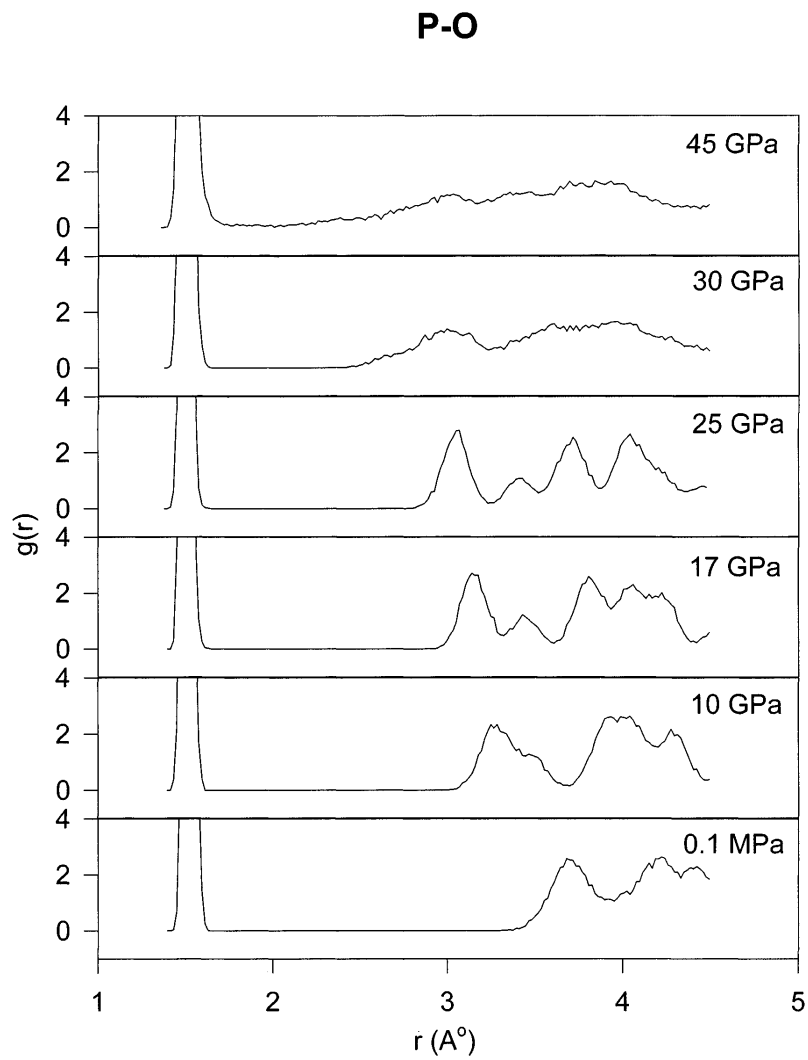

(b)

Figure 3. (Continued)

the Al–O radial distribution function $g(r)$. This minimum is mostly stable at ∼2.4 Å. Around 30 GPa, Al–O coordination increases to ∼5.2 and beyond this pressure it gradually increases to 5.8 at 65 GPa. In contrast, Tse and Klug [11] found that Al is six coordinated to oxygen atoms at about 40 GPa. It is possible that these differences are due to a choice of somewhat different coordination radii used by others [10, 11]. We find that P–O coordination increases to 4.75 at 65 GPa while Tse and Klug found it to increase to 4.6 by 80 GPa. Figure 3 shows the pressure induced changes in the radial distribution function $g(r)$ for Al–O, P–O and O–O.

Powder x-ray diffraction patterns were constructed from the averaged coordinates at each pressure to look for any change that could be discerned by the x-ray diffraction technique. This method has been successfully used earlier for determining a new high pressure structure of α-quartz [30]. For $AlPO_4$ some calculated diffraction patterns are shown in figure 4.

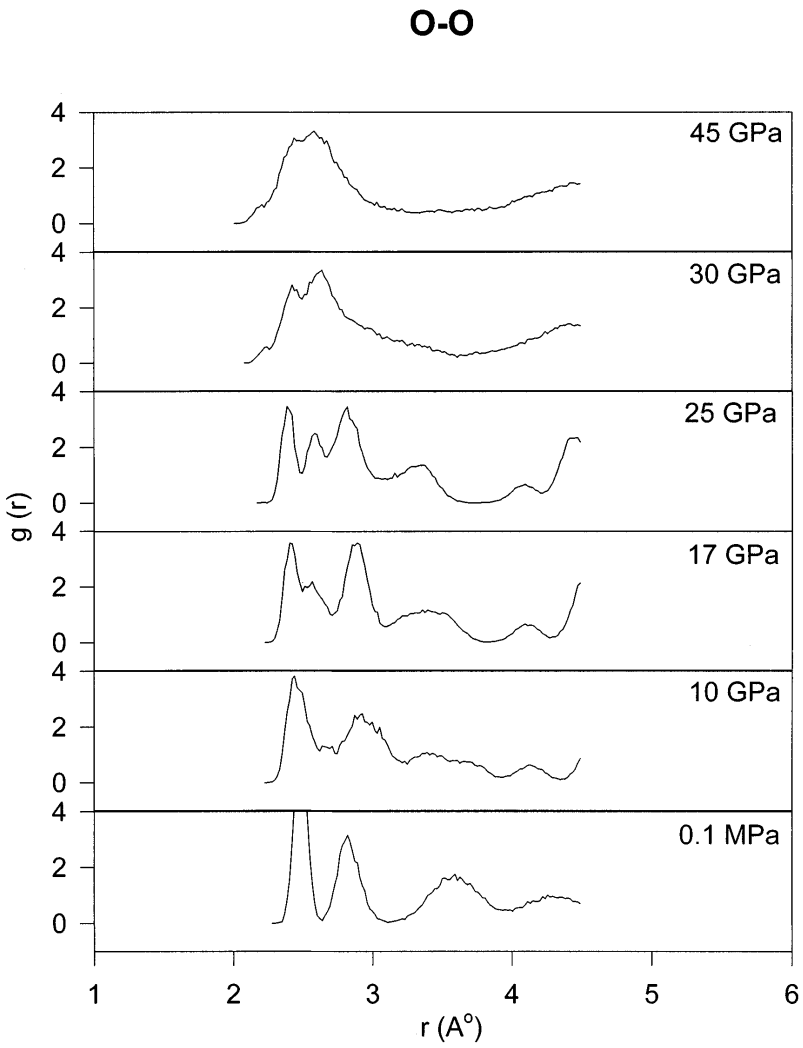

(c)

Figure 3. (Continued)

The diffraction pattern at 0.1 MPa is completely indexed with the unit cell of the berlinite phase. All the observable diffraction peaks display systematic and monotonic shifts with pressure up to 30 GPa. However as some d_{hkl} shift more than the others, some peaks merge and split again around 7 GPa. As this is a simple consequence of cross-over of various d we cannot categorize this as a phase transformation. Hence, we do not find any evidence for a phase transformation at 6.5 GPa [16]. We also note that at ∼15 GPa, the intensities of the diffraction peaks reduce to almost half the value at 0.1 MPa. In addition, beyond 30 GPa, the intensities of many Bragg peaks diminish abruptly. The calculated diffraction pattern does not show any superlattice diffraction peaks corresponding to the tripling of unit cell in the basal plane, as expected from softening of just one zone boundary mode [8, 9, 12]. At pressures higher than ∼45 GPa only two remaining peaks can be clearly seen while the intensity of all others is such that it may be characterized to be x-ray amorphous. The indices of remaining peaks are $(10\bar{1}2)$ and $(10\bar{1}4)$

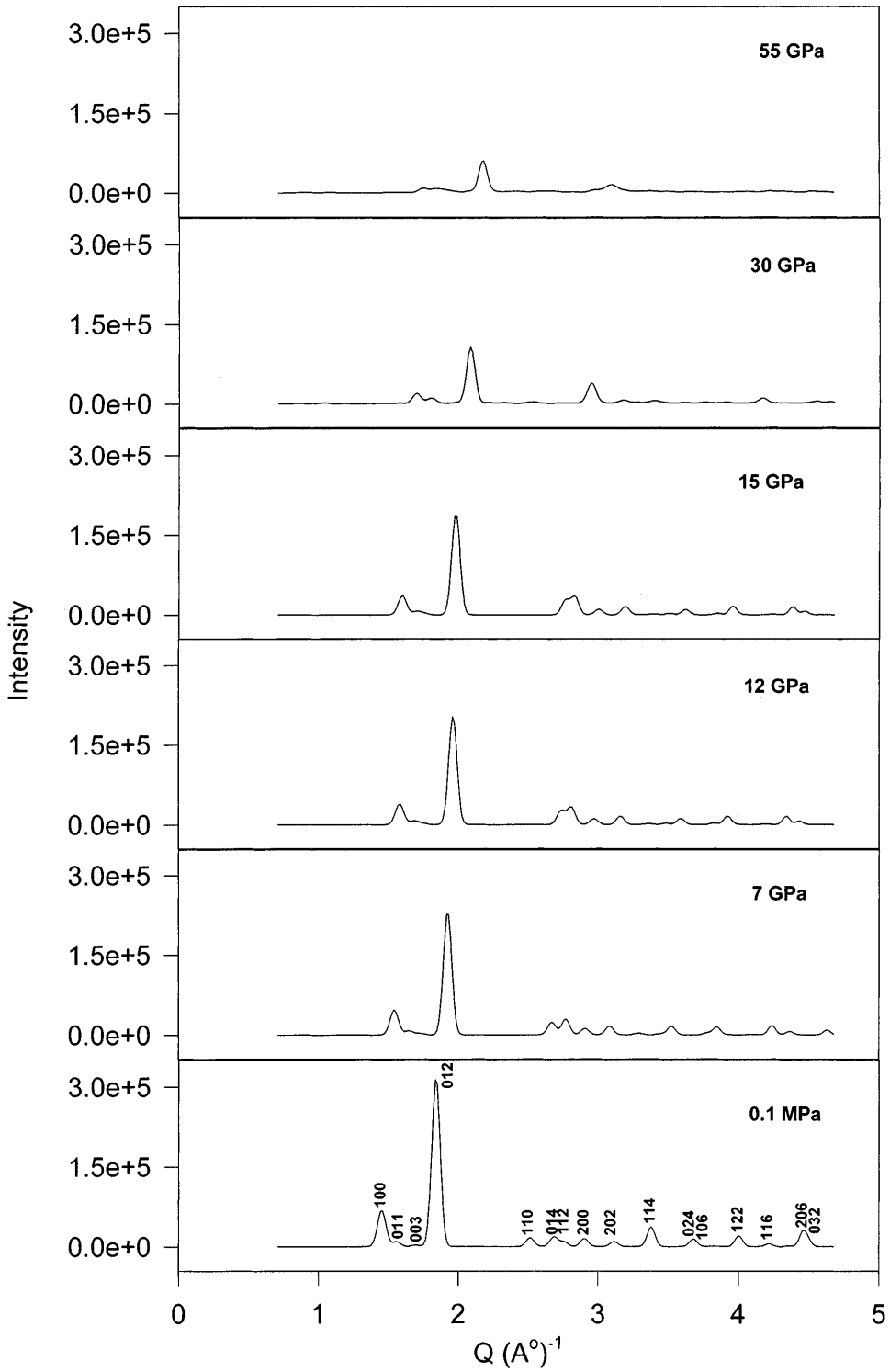

Figure 4. Computed diffraction patterns from equilibrated atomic positions in $AlPO_4$ at various pressures.

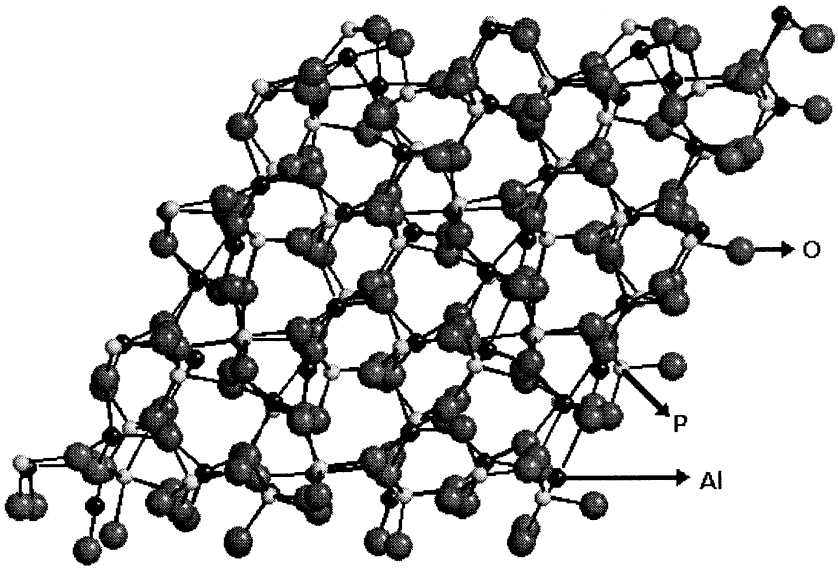

(a)

Figure 5. The structure of the disordered phase of $AlPO_4$ at 45 GPa (a) along the c-axis, (b) along the (010) axis. (c) The structure of $AlPO_4$ at 15 GPa along the (010) axis.

when indexed with the unit cell of the α-phase. Some residual diffraction peaks have also been noted to exist in the MD calculations of Tse and Klug [11]. However, these authors ignored the existence of these diffraction peaks and concluded amorphization of $AlPO_4$ beyond 30 GPa. To understand the persistence of diffraction peaks beyond 30 GPa, we analysed the structure from various crystallographic directions. Figures 5(a) and 5(b) show the two views of the atomic arrangement in $AlPO_4$ at 45 GPa. The one along the c-axis suggests the formation of a disordered phase. However, the view along (010) direction indicates the existence of a remnant translational order that is responsible for the residual diffraction peaks. This remnant translational order along (010) is considerably different from what is observed in the structure beyond 15 GPa (figure 5(c)). However, due to the concomitant disorder it is difficult to quantify the remnant translational order except by the intensity of the residual diffraction peaks. Here, it is also interesting to note that under shock loading, berlinite amorphizes in the lamellae whose habit planes are $(10\bar{1}n)$. Similar results in shock loaded quartz have been explained in terms of instabilities of shear modulus in these planes [31].

The P–V/V_0 curve in figure 1 does not show any first order phase transformation around 12–15 GPa. However, the calculated c/a ratio displays a change of slope as shown in figure 6. At lower pressures the calculated c/a is in fair agreement with the experimental observations [29]. The compression along the $\boldsymbol{c}$ and $\boldsymbol{a}$ axis is found to be anisotropic up to $\sim$12 GPa. However, beyond this pressure the linear increase in c/a ratio reduces and forms a plateau. This loss of anisotropy could be due to the distortion of the tetrahedral network as discussed in section 3.1.2. To understand the evolution of structure in this pressure range, we first note that between 10 and 15 GPa, $g(r)$ in figure 3 suggest atomic reordering between 2.8 and 4.2 Å. However, these variations give no idea about the nature of new arrangements. As the calculated diffracted intensity diminishes at $\sim$15 GPa, we looked for any signatures of possible disordering. For this, we carefully analysed the atomic translational order for each of Al, P and O atoms. Analyses showed that the oxygen atoms are disordered while there is no substantial

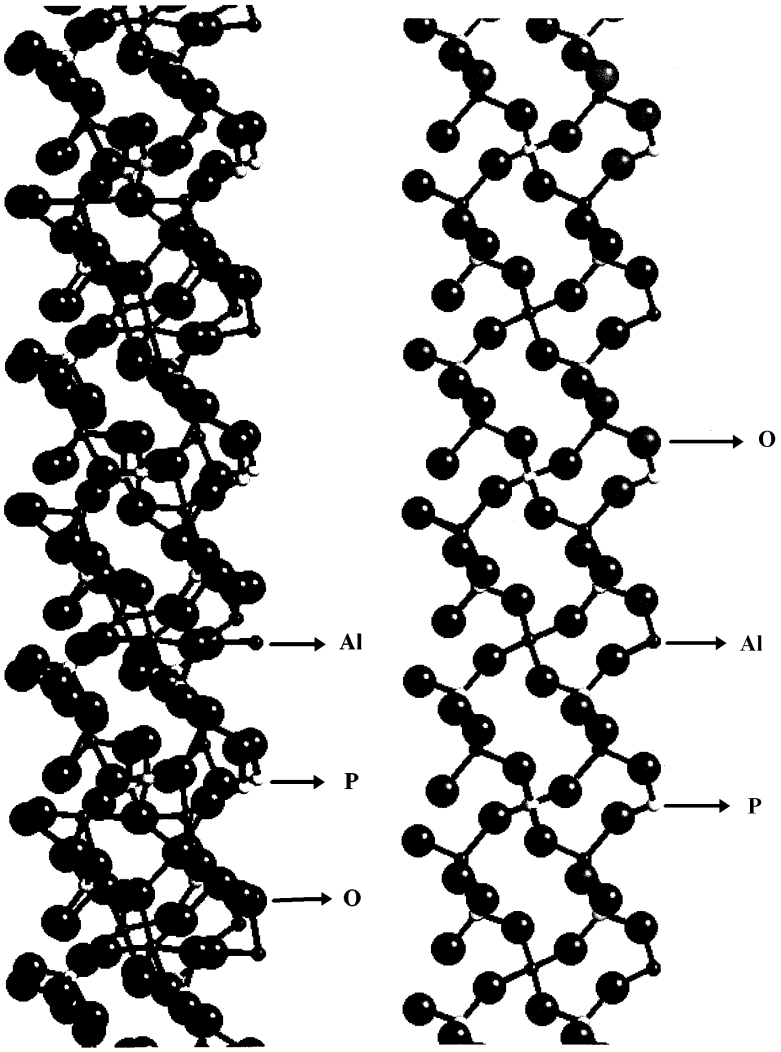

(b) (c)

Figure 5. (Continued)

disordering of the Al and P atoms. A confirmation of this is the diffraction pattern generated by only oxygen atoms as shown in figure 7(a). For comparison, the partial diffraction patterns generated from only Al and P are also shown in figures 7(b) and 7(c) respectively. Figure 7(a) shows a fall in the Bragg diffracted intensity at 12 GPa to one third of its initial value at 0.1 MPa. This is particularly clear from a non-overlapping (012) peak. This disordering of oxygen atoms supports the suggestion of Gillet *et al* [13] who find that around this pressure, berlinite transforms to a disordered crystalline phase. This also agrees with the single crystal x-ray diffraction results of Sun *et al* [17]. Further, as shown in figure 2, at this pressure Al–O and P–O coordination is still four. Absence of higher Al–O coordination at this pressure suggests that the structure of $AlPO_4$ at $\sim$15 GPa cannot be a mixture of the *Cmcm* and the p-glass phases [20].

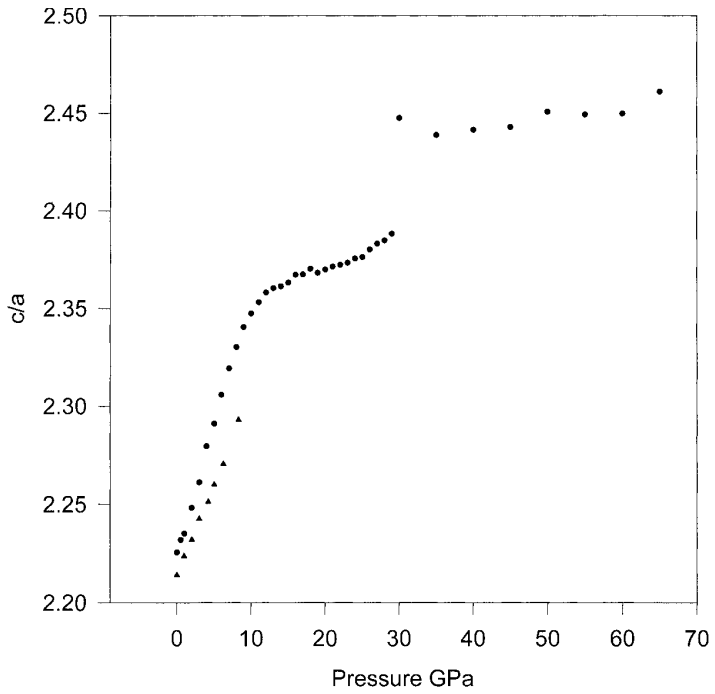

Figure 6. Calculated variation of c/a of $AlPO_4$ as a function of pressure; triangles represent the experimental points from [29].

3.1.2. Nature of tetrahedral distortion. To understand the pressure induced deformation of AlO_4 and PO_4 tetrahedra in quantitative terms we have analysed the microscopic distortions in terms of quadratic elongation and variance of tetrahedral or octahedral angles [32]. The former is a measure of T–O (T = Al or P) bond length variation in a constituent polyhedron while the latter indicates the angular distortion with respect to that of an ideal polyhedron. We use these parameters as defined by Robinson *et al* [32], which for tetrahedral complexes are as follows,

$$\lambda_{tet} = \frac{1}{4}\sum_{i}^{4}\left(\frac{l_i}{l_0}\right)^2 \tag{1}$$

$$\sigma_\theta(\text{tet}) = \frac{1}{5}\sum_{i}^{6}(\theta_i - 109.47)^2 \tag{2}$$

where l_i represents the actual bond length compared to the ideally equal bond lengths l_0, and θ_i represents various OTO angles of the tetrahedra. λ_{tet} and σ_θ(tet) were computed for all the tetrahedra in the MD cell and are plotted in figure 8 for $P = 15$ GPa. Calculated λ_{tet} and σ_θ(tet) display a strong linear correlation, similar to what is known for various naturally occurring minerals [32]. We find that for $AlPO_4$ the slope of quadratic elongation versus angle variance is almost same for AlO_4 and PO_4 tetrahedra, however this slope is slightly larger than that for the natural silicate and aluminosilicate minerals [32]. Variation of this slope as a function of pressure is shown in figure 9. This slope decreases up to 15 GPa and beyond this pressure, it increases. This feature, though it may not necessarily imply a phase transition at ∼15 GPa, is more probably a signature of the disordering of oxygen atoms at ∼15 GPa.

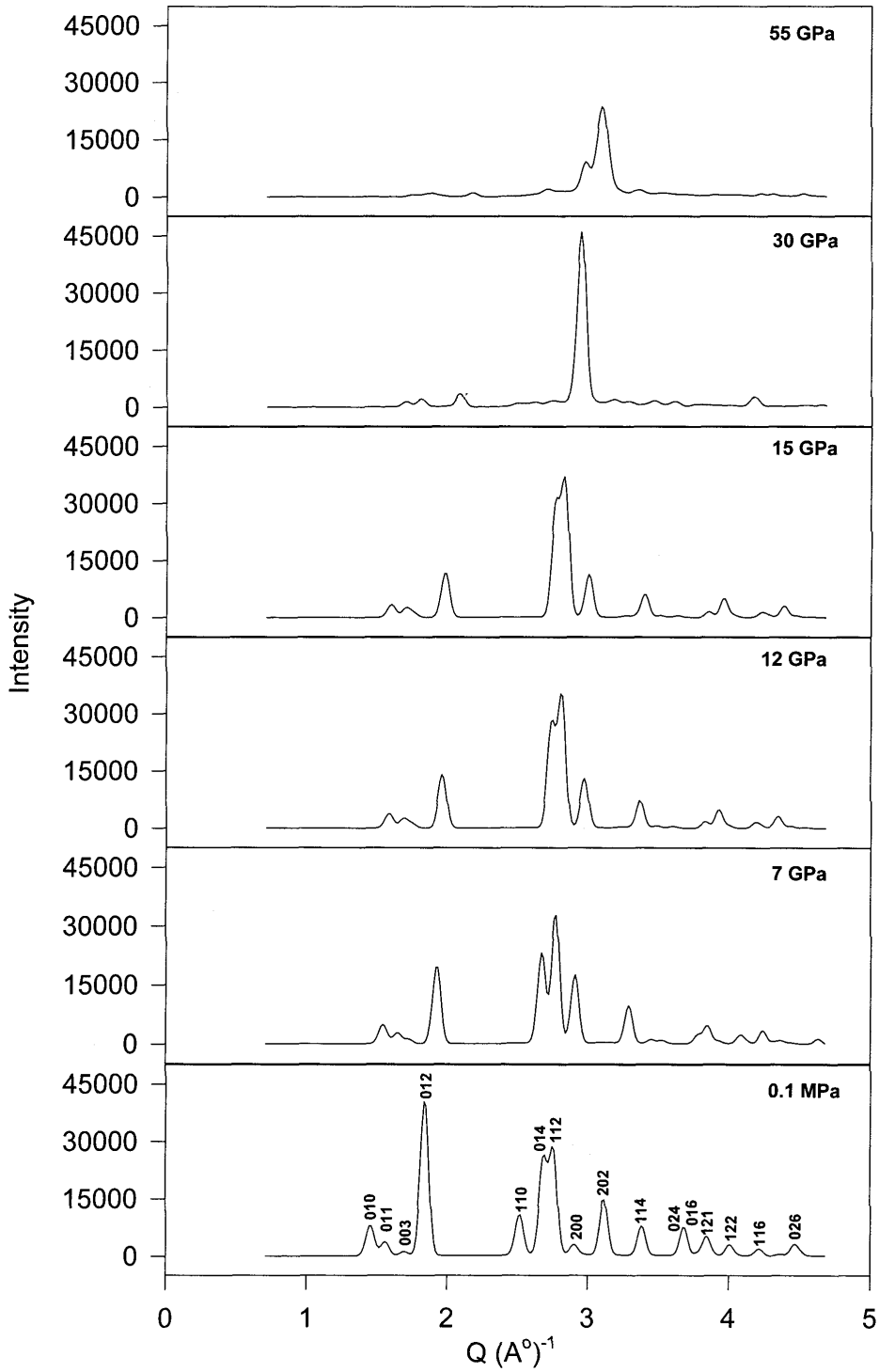

(a)

Figure 7. Calculated partial diffraction patterns from only (a) oxygen atoms, (b) aluminum atoms and (c) phosphorus atoms at various pressures.

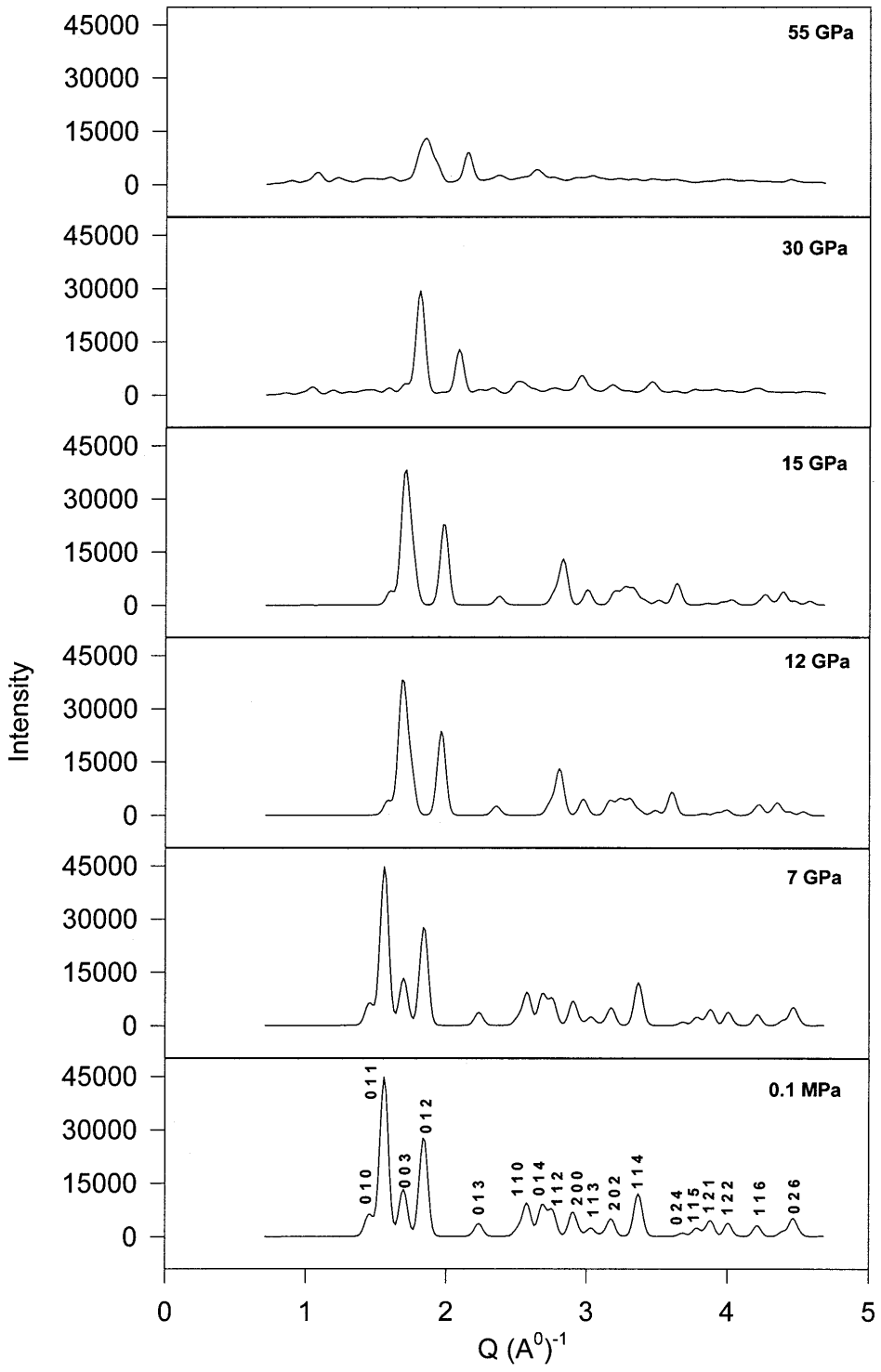

(b)

Figure 7. (Continued)

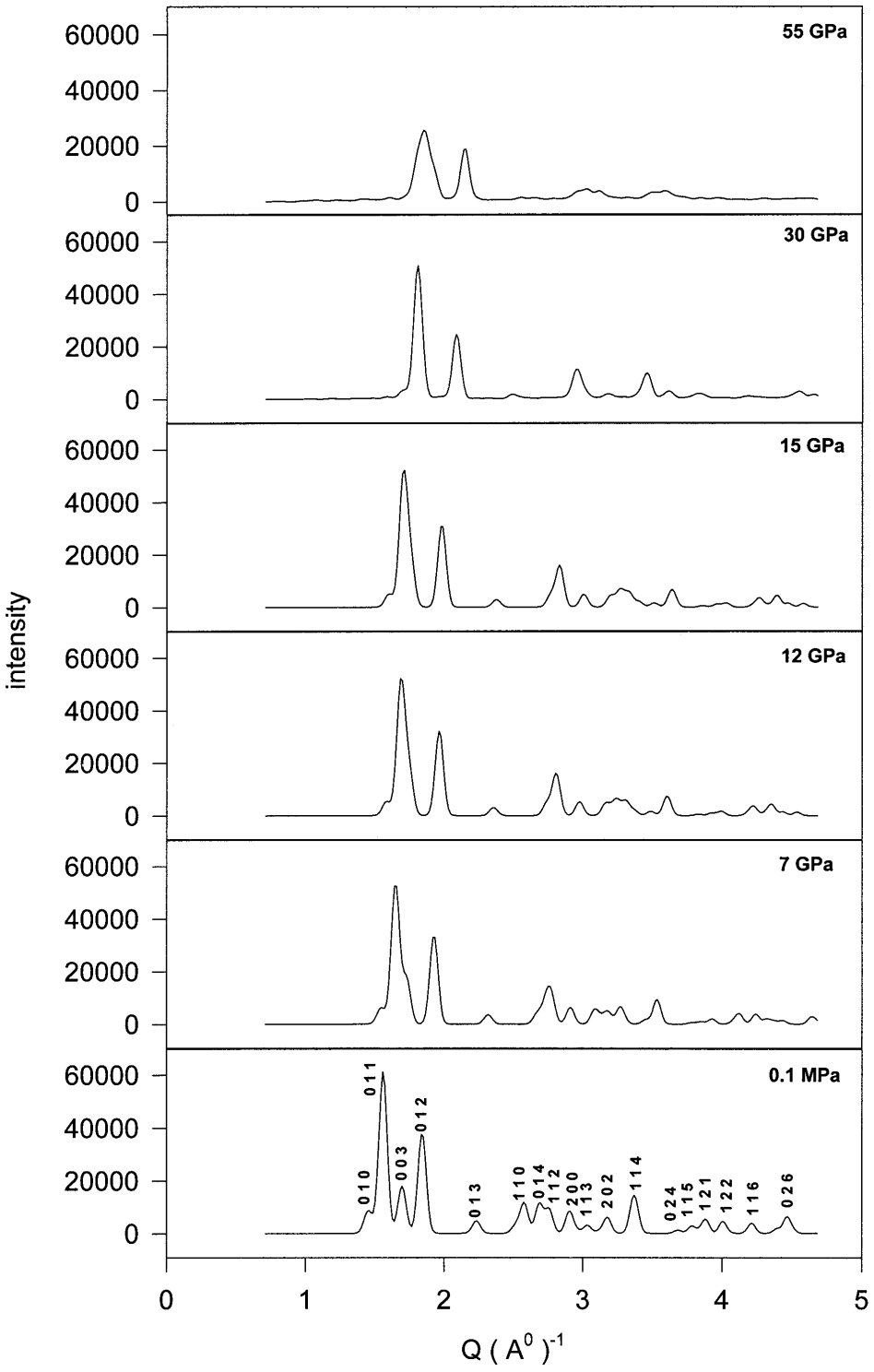

(c)

Figure 7. (Continued)

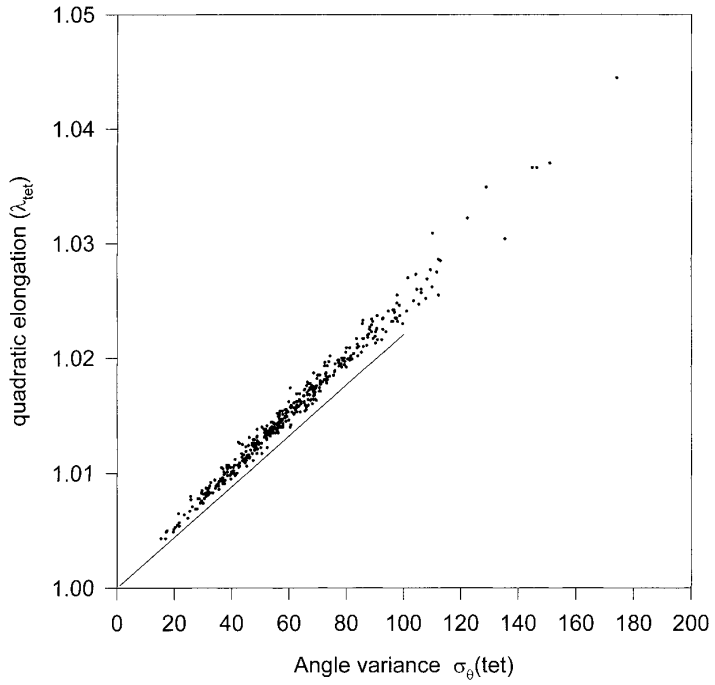

Figure 8. Variation of average quadratic bond elongation variance with angle variance in AlO_4 and PO_4 tetrahedra of $AlPO_4$ at 15 GPa.

Figure 10 presents the angular deformation of both AlO_4 and PO_4 tetrahedra in terms of distribution of angular variance defined above [33]. Even at 0.1 MPa, AlO_4 tetrahedra show higher angular variance than PO_4. At higher pressures, the angle variance of PO_4 tetrahedra undergoes a systematic shift from lower to higher values, which gives a higher average value. However, the distribution continues to be localized to a band of (20–60). In contrast, AlO_4 shows relatively larger spread. Even at 11 GPa the distribution of angle variance is over (40–100) and by 18 GPa, it further increases to (40–120). Averaged angle variance over the whole MD cell shows a monotonic increase with pressure, changing from ∼10 to 50 for PO_4 and 25 to 100 for AlO_4 as the pressure increases to 30 GPa. This systematic increase of variance implies that the deformation of the tetrahedra does not appear suddenly close to the pressure of the first order phase transition to a disordered phase. Instead it grows gradually and at ∼30 GPa the existence of large tetrahedral deformations may be responsible for the transformation of the crystalline phase to a disordered phase.

3.1.3. Steric hindrances and phase transitions. Analyses of several experimental and theoretical results establish that the pressure induced amorphization is brought about by the structural frustration caused by kinetic impedance and steric hindrances [7, 34, 35]. The steric constraints arise due to the reduction of non-bonded inter-atomic distances under pressure, when a significant modification of the molecular shapes is kinetically inaccessible. However, these non-bonded inter-atomic distances cannot be reduced arbitrarily. At some compression, these will reach a limiting value. In fact, now it is well known that there is a general correlation between the pressures of phase transformations and the limiting distances of non-bonded atoms [7, 34, 35]. Physically this is due to the fact that the repulsive energy cost for further squeezing

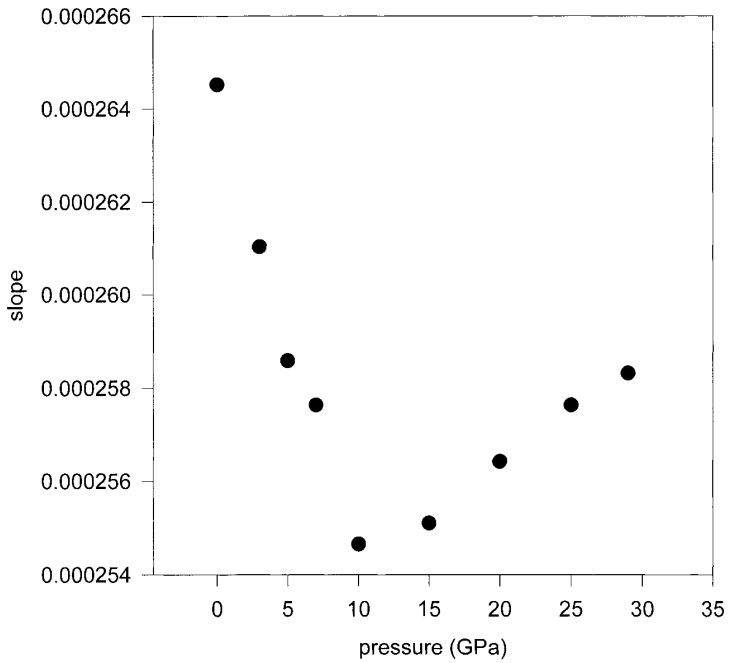

Figure 9. Variation of slope of quadratic bond elongation variance with angle variance of AlO_4 and PO_4 tetrahedra of $AlPO_4$ as function of pressure.

these non-bonded atoms far exceeds the energy cost of distortion of polyhedra. This leads to a phase transition to relieve the steric strain in the structure [35]. Some typical limits of these non-bonded distances have been listed in [7]. For $AlPO_4$ the relevant distances are for the non-bonded O···O atoms. For these the largest steric limit is Pauling's van der Waals separation of 2.8 Å and the smallest extreme limiting value is 2.6 Å. Generally, at the upper limit of these distances polyhedral distortions start and these distortions reach a maximum when the extreme limiting distance is reached [7, 36]. In an earlier MD calculation [12], it was found that in $AlPO_4$, the O···O distances, evaluated from a single crystallographic unit cell, reach a limiting value of 2.8 Å at ∼30 GPa. However, a survey of several examples [7, 35], suggests that generally a phase transformation is not initiated at the van der Waals limiting distance.

Now we have recalculated the variation of the non-bonded O···O distances and this is as plotted in figure 11. These non-bonded distances were generated from the central $2 \times 2 \times 2$ part of the MD cell. All shortest non-bonded distances were calculated and it was observed that there is a considerable amount of statistical variation and this variation is shown as error bars in figure 11. The O···O distances decrease with pressure and between ∼10 and 15 GPa these reach a plateau value of ∼3 Å. (Coincidentally this partly overlaps with the pressure range where c/a shows a plateau.) However, even at these average values, there are quite a few O···O contacts which are close to ∼2.8 Å, which is the first limiting distance for non-bonded oxygen atoms. Apparently the nature of tetrahedral distortions at 15 GPa is such that it permits further shortening of O···O distances. At 29 GPa, though the average O···O is ∼2.78 Å; there are a few O···O contacts where distances are as small as 2.58 Å i.e. these are near the extreme limit of 2.6 Å. It is quite likely that the tetrahedra related to extreme limiting distances are the nucleating sites of the disordered phase.

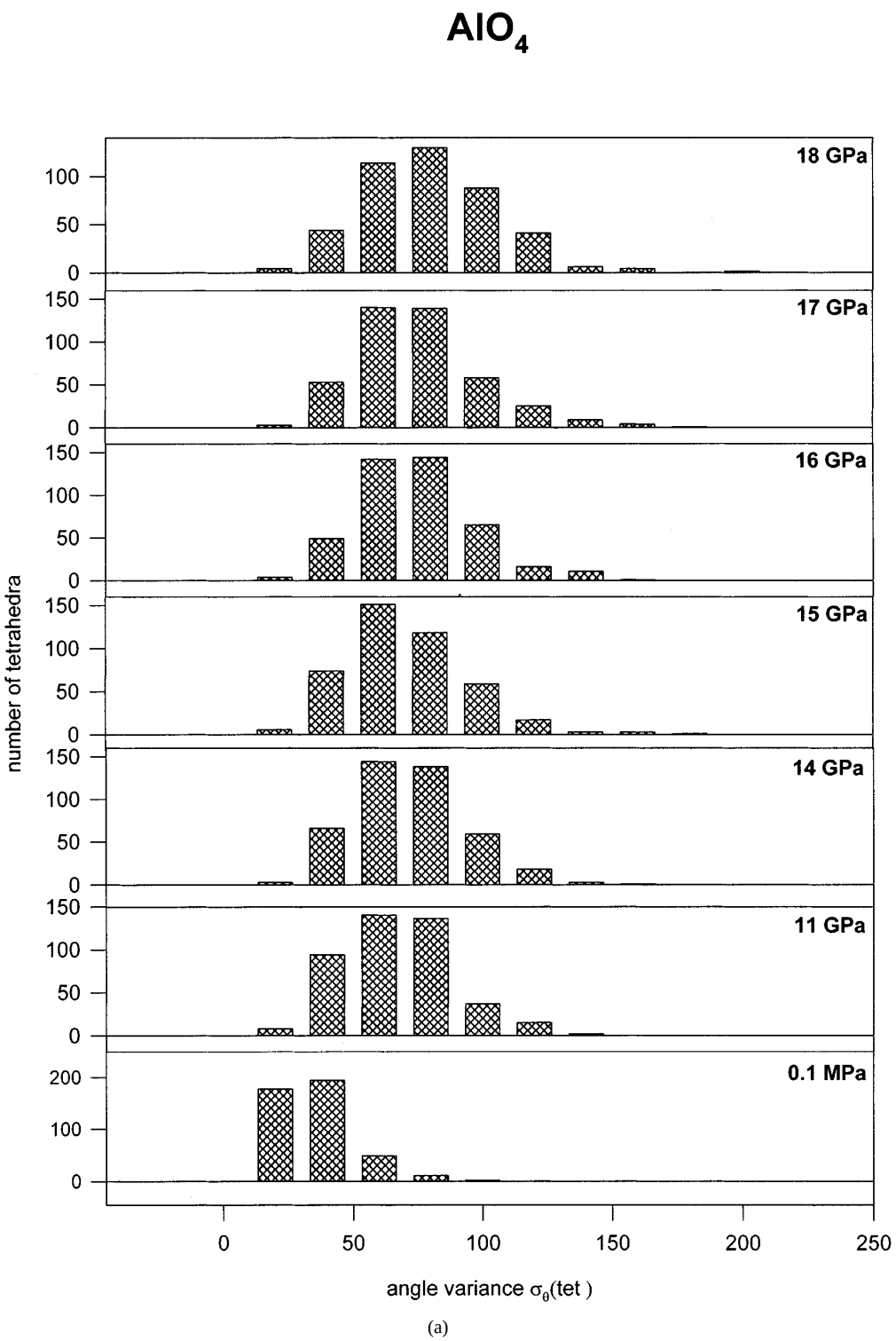

(a)

Figure 10. Histograms showing the spread of angle variance of tetrahedra of $AlPO_4$ at various pressures. (a) AlO_4 (b) PO_4.

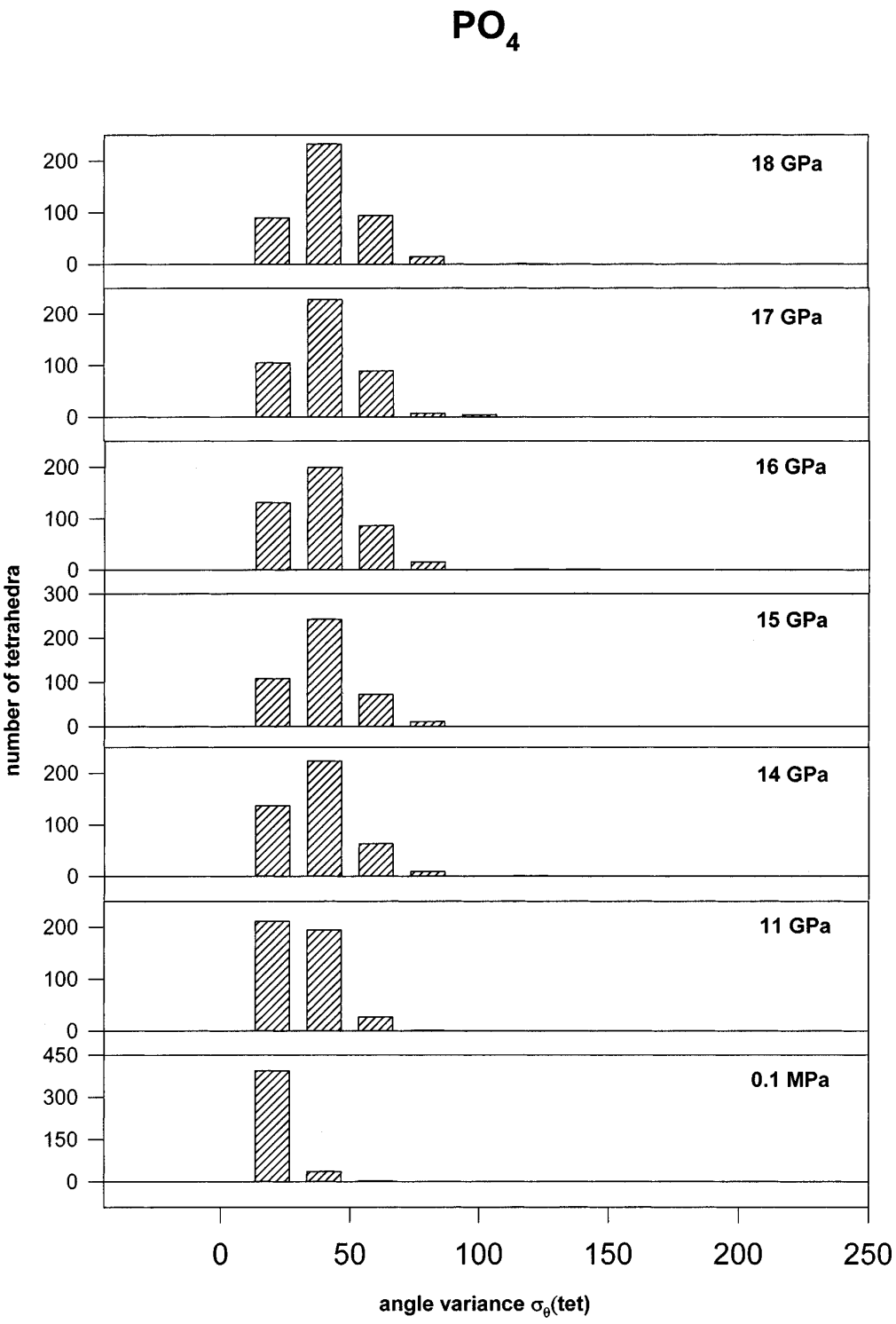

(b)

Figure 10. (Continued)

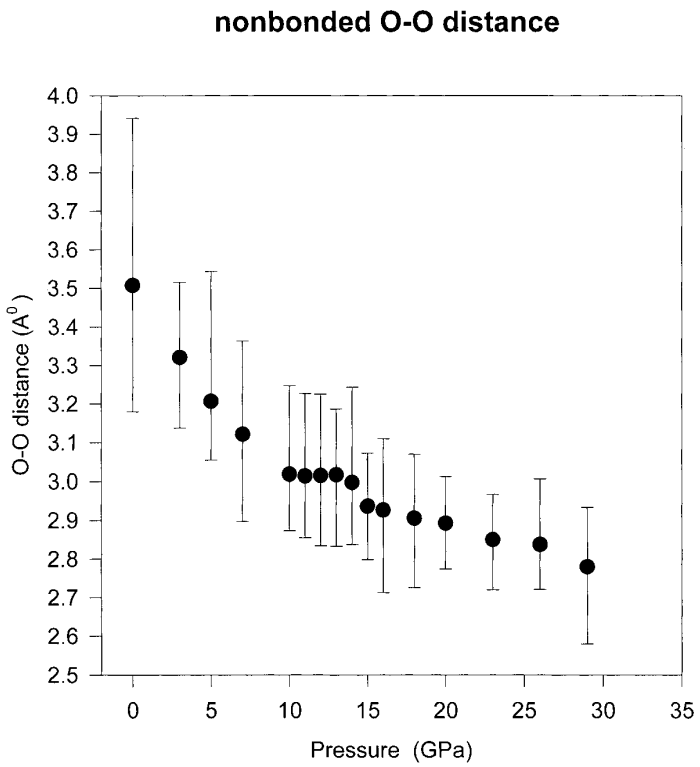

Figure 11. Variation of non-bonded O···O distances as a function of pressure. The error bars indicate the smallest and the largest O···O distances within the central $2 \times 2 \times 2$ part of the MD cell.

3.2. Phase transformation to another crystalline phase

3.2.1. Annealing at high pressures. First we consider annealing at 20 GPa. We mentioned in section 1 that Raman scattering results of Gillet *et al* indicate a crystalline to (disordered) crystalline phase transformation at ∼14 GPa [13]. Therefore, at 20 GPa we slowly raised the temperature of the partially disordered crystalline phase to 2000 K. The purpose of this annealing was to overcome any kinetic barrier to a transformation to the *Cmcm* phase or any other crystalline phase. Our calculated diffraction pattern of $AlPO_4$ as well as of the oxygen sublattice continues to show the same kind of disorder as at 300 K. Therefore, our simulations do not support the transformation of the partially disordered phase that exists between 15 and 30 GPa to any other crystalline structure.

Next, we discuss annealing at 45 GPa. In an earlier simulation [12] the amorphous phase at 35 GPa was heated to 2000 K to search for the *Cmcm* phase. We note from figure 4 that the phase at 35 GPa is not fully (x-ray) amorphous and that it requires a substantially higher compression. In addition, in the *Cmcm* phase Al–O coordination is required to be six. Therefore, a higher pressure is likely to be more favourable for crystallization of this phase. Hence we annealed the disordered phase at 45 GPa up to 2000 K. Our results find no evidence of any atomic reordering which may indicate an approach of a crystalline phase. Therefore, we conclude that with the pair potentials of van Beest *et al*, even at 45 GPa and 2000 K, the disordered phase is a kinetically preferred state.

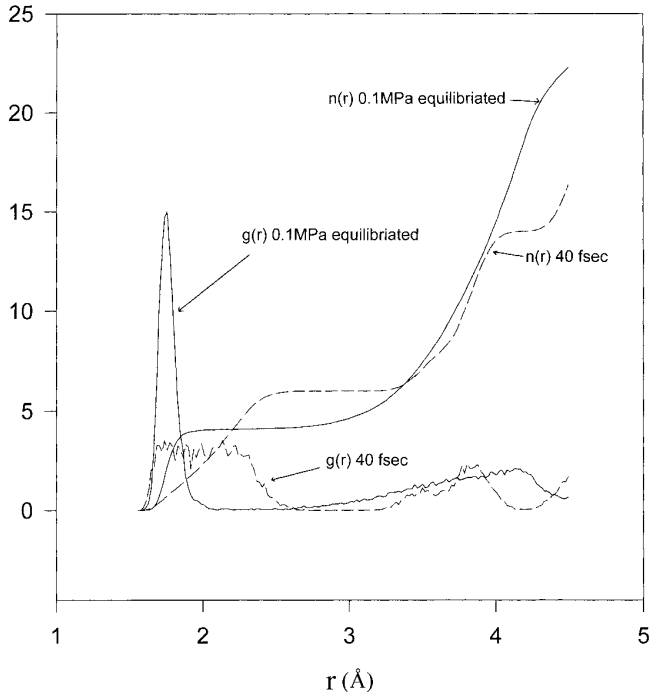

Figure 12. Time evolution of Al–O coordination when simulations start from *Cmcm* phase. The dashed line represents the radial distribution function $g(r)$ and Al–O coordination number $n(r)$ after 40 fs. We note that on equilibration the starting phase of six (Al–O) coordination transforms to a four coordinated state indicating a clear preference for the latter at ambient conditions. This implies that the *Cmcm* phase can not be retained metastably at ambient conditions.

3.2.2. Simulation of $AlPO_4$ in the Cmcm phase. As mentioned in the introduction, earlier calculations [12] as well as experiments in isomorphous materials [18–20] suggest a possibility of a transformation to the *Cmcm* phase; we have carried out somewhat different computations on $AlPO_4$ in the *Cmcm* phase. In these calculations the starting structure of $AlPO_4$ is taken to be *Cmcm*. As in our calculations we use the NPT dynamics with Melchionna's modifications, we can evaluate the issue of relative stability of the α-phase and the *Cmcm* phases in terms of total energy [37]. For these simulations the starting orthorhombic structure is same as described earlier in section 2. Equilibration at 0.1 MPa, 300 K results in a disordered structure. Figure 12 shows that with the starting atomic coordinates of the *Cmcm* phase, Al–O coordination continues to be six for several time steps. However, on equilibration, although the volume per formula unit decreases, the Al–O coordination becomes four, indicating a clear preference for a four coordinated structure at low pressures. Structurally this four coordinated phase is found to be disordered. This disordered phase was pressurized slowly up to 65 GPa to explore the possibility of its transformation back to the *Cmcm* phase at some higher pressure. However, the disordered phase continues to persist up to 65 GPa. The total energy of the *Cmcm* disordered phase is found to be higher than that of the α-phase as well as the high pressure disordered phase emerging from the α-phase. To evaluate whether this *Cmcm* disordered phase is metastably trapped, we heated this phase to 2800 K at 20 GPa, i.e. at a pressure where earlier enthalpy considerations had indicated that the *Cmcm* phase is more stable. This annealing further increases the disorder in this phase and does not show any indication of an emerging

crystalline order. These results imply that under hydrostatic pressures, pair potentials of van Beest *et al* [22] do not favour a fast enough dynamical path for the formation of the *Cmcm* phase or the α-phase from this new disordered phase.

3.2.3. Sudden high pressure loading of the Cmcm phase. Failure to observe the *Cmcm* phase in $AlPO_4$ through various simulations mentioned above may indicate that this transformation is perhaps too sluggish to be seen in the MD simulations. In addition, we find that the *Cmcm* phase is not metastable at ambient conditions. These two aspects represent the basic difficulty in the investigation of the *Cmcm* phase through MD calculations despite the fact that the enthalpy favours this phase beyond 12 GPa. To arrest the decay of the *Cmcm* phase we carried out simulations where this phase is instantaneously subjected to high pressures. This may be viewed as a simulation of shock response of a hypothetical *Cmcm* phase dispersed in an ideal elastomer (fluid-like environment). Experimentally this kind of shock loading of materials in an elastomer is routinely carried out to facilitate a comparison of the shock results with those under static compression [38]. For this simulation we started with the atomic coordinates representative of the *Cmcm* phase, as described in section 3.2.2, but the pressure was suddenly increased from 0.1 MPa to several GPa. We find that below a final pressure of 20 GPa the *Cmcm* phase does not stabilize. However this sudden pressure loading to 20 GPa traps the *Cmcm* phase. We also observe that despite this fast external pressure loading, the internal pressure stabilizes within $\sim$11 ps to 20 GPa. Also the total energy of this *Cmcm* phase is found to be lower than that of the α-phase as well as the *Cmcm* glass. On back-extrapolation we find that the total energy of the *Cmcm* phase becomes equal to that of the berlinite phase around 12 GPa. Despite the lack of stability of the *Cmcm* phase below 20 GPa, the extrapolated equality of the energies at $\sim$12 GPa confirms the earlier conclusions based on enthalpy calculations. In addition, this shows that the results of these simulations are physically reasonable. Time evolution of the stress tensor showed the existence of large off-diagonal components before equilibration to the final cell dimensions in the *Cmcm* phase. Therefore, we feel that the stabilization of the *Cmcm* phase on sudden pressure loading may be aided by the existence of non-hydrostatic stresses. Therefore, one may speculate that it may be possible to access the *Cmcm* phase under non-hydrostatic stresses, either under static or under dynamic pressure loading. And *if* shock loading and/or non-hydrostatic stress loading of the α-phase leads to a *Cmcm* phase then our simulations suggest that on recovery one may observe the glassy phase (as experimentally found! [4]) which arises from the *Cmcm* phase. In the light of results of section 3.2.2, this amorphous phase will not be the same as the high pressure disordered phase. More experiments and simulations under non-hydrostatic stresses may help settle this issue.

4. Conclusions

The results of our MD simulations presented here do not show the existence of any phase transition below 10 GPa. The changes observed around 15 GPa are subtle and continuous and represent growing tetrahedral distortion. Our results at $\sim$15 GPa indicate that the structure is not amorphous but has oxygen sublattice disorder and support the Raman measurements of Gillet *et al* [13] and x-ray diffraction results of Sun *et al* [17]. The suggestion that berlinite transforms to a new crystalline phase close to 15 GPa is not supported by our results. Even though we observe, as in earlier calculations, a first order phase transformation at $\sim$30 GPa, the calculated diffraction pattern shows that this phase is highly disordered but not amorphous. Some diffraction peaks continue to persist up to $\sim$60 GPa. These results should encourage careful x-ray diffraction experiments to settle some of these issues unambiguously. Further,

because in principle, *Cmcm* phase is of lower energy, it may be possible to reach this phase through other kinds of loading such as under non-hydrostatic stresses or under shock loading.

Acknowledgment

The authors are grateful to Dr S K Sikka for his critical comments, illuminating discussions and suggestions on several aspects of the MD simulations presented in this manuscript.

References

[1] Kruger M B and Jeanloz R 1990 *Science* **249** 647
[2] Sankaran H, Sharma S M, Sikka S K and Chidambaram R 1990 *Pramana J. Phys.* **35** 177
[3] Somayazulu M S, Garg N, Sharma S M and Sikka S K 10994 *Pramana J. Phys.* **43** 1
[4] Cordier P, Gratz A J, Doukhan J C and Nellis W J 1994 *Phys. Chem. Miner.* **21** 133
[5] Cordier P, Doukhan J C and Peyronneau J 1993 *Phys. Chem. Miner.* **20** 176
[6] Polian A, Grimsditch M andPhilippot E 1993 *Phys. Rev. Lett.* **71** 3143
[7] Sharma S M and Sikka S K 1996 *Prog. Mater. Sci.* **40** 1
[8] Keskar N R, Chelikowsky J R and Wentzcovitch R M 1994 *Phys. Rev.* B **50** 9072
[9] Watson G W and Parker S C 1995 *Phys. Rev.* B **52** 13 306
[10] Vessal B 1991 *Trans. Am. Cryst. Assoc.* **27** 37
[11] Tse J S and Klug D D 1992 *Science* **255** 1559
Tse J S and Klug D D 1991 *Phys. Rev. Lett.* **67** 3559
Singh A K (ed) 1992 *Recent Trends in High Pressure Research* (New Delhi: IBH) p 274
[12] Chaplot S L and Sikka S K 1993 *Phys. Rev.* B **47** 5710
Singh A K (ed) 1992 *Recent Trends in High Pressure Research* (New Delhi: IBH) p 259
[13] Gillet P, Badro J, Varrel B and McMillan P F 1995 *Phys. Rev.* B **51** 11 262
[14] Jayaraman A, Wood D L and Maines R G 1987 *Phys. Rev.* B **35** 8316
[15] Woulf *et al* unpublished, quoted in [13]
[16] Kruger M B and Meade C 1994 *Bull. Am. Phys. Soc.* N30 1, p 667
[17] Sun T, Herbst C, King H E Jr and Kruger M 1994 *Bull. Am. Phys. Soc.* N302, p 668
[18] Pasternak M P, Rozenberg G Kh, Milher E, Amanowicz M, Zhou T, Schwarz U, Syassen K, Taylor R D and Hanfland M 1997 *Phys. Rev. Lett.* **79** 4409
[19] Murli C, Sharma S M, Kulshreshtha S K and Sikka S K 1997 *Pramana J. Phys.* **49** 285
[20] Badro J, Itie J P and Polian A 1998 *Eur. Phys. J.* B **1** 265
[21] The behaviour of berlinite under non-hydrostatic stresses in a diamond anvil cell [5] as well as under shock loading [4] is different from that under hydrostatic pressures. In this case, material is partially converted into an amorphous phase, in the form of thin lamellae parallel to $\{10\bar{1}n\}$ planes [4, 5]. However as our MD simulations deal only with hydrostatic pressures, the discussion of the non-hydrostatic case is beyond the scope of this investigation.
[22] van Beest B W H, Kramer G J and van Santen R A 1990 *Phys. Rev. Lett.* **64** 1955
[23] Smith W and Forester T R 1996 Copyright Council for Central Laboratory of Research Councils, Daresbury Laboratory at Daresbury, Nr Warrington, UK
[24] Melchionna S, Ciccotti G and Holian B L 1993 *Mol. Phys.* **78** 533
[25] Hoover W G 1985 *Phys. Rev.* A **31** 1695
[26] Thong N and Schwarzenbach S 1979 *Acta Crystallogr.* A **35** 658
[27] Wyckoff R W G 1964 *Crystal Structures* 2nd edn (New York: Interscience)
[28] Kramer G J, van Beest B W H and van Santen R A 1991 *Phys. Rev.* B **43** 5068
[29] Sowa H, Macavei J and Schulz H 1990 *Z. Kristallogr.* **192** 119
[30] Somayazulu M S, Sharma S M and Sikka S K 1994 *Phys. Rev. Lett.* **73** 98
[31] Goltrant O, Leroux H, Doukhan J C and Cordier P 1992 *Phys. Earth Planet. Inter.* **74** 219
[32] Robinson K, Gibbs G V and Ribbe P H 1971 *Science* **172** 576
[33] We could have chosen to present this distribution as a function of standard deviation, and one may deduce one, by replacing the values on the abscissa by the square root of the variance. However, the advantage of retaining our plots in terms of variance is that one can obtain a closely related graph in terms of quadratic elongation by multiplying the variance by the slope from figure 9.
[34] Sikka S K and Sharma S M 1992 *Curr. Sci.* **63** 317

[35] Sikka S K, Sharma S M and Chidambaram R 1994 *High Pressure Science and Technology—1993* ed S C Schmidt, J W Shaner, G A Samara and M Ross (New York: AIP) p 213

[36] Calculations using interatomic potentials for non-bonded interactions indicate that the limiting non-bonded separation corresponds to a repulsive energy of almost 4–5 kJ mol^{-1} [7]. (See also Sikka S K 1997 *Ind. J. Pure Appl. Phys.* **35** 677). This energy is comparable to the typical free energy differences between different polymorphs of a substance and therefore provides a rationale for the system to undergo a phase transformation.

[37] The computed total energy is the total internal energy of the system which includes all contributions to the energy (including system extensions due to thermostats etc). It is nominally the conserved variable of the system and represents equation (14) of [24].

[38] Tang Z P and Gupta Y M 1988 *J. Appl. Phys.* **64** 1827